

Article

Sixty-Nine-Element Voice Coil Deformable Mirror for Visible Light Communication

Lv Jiang ^{1,2} , Lifa Hu ^{1,2}, Qili Hu ³, Xingyu Xu ^{1,2}, Jingjing Wu ^{1,2}, Lin Yu ^{1,2} and Yang Huang ^{1,2,*} 

¹ School of Science, Jiangnan University, Wuxi 214122, China; 6201201008@stu.jiangnan.edu.cn (L.J.); hulifa@jiangnan.edu.cn (L.H.); 6211205027@stu.jiangnan.edu.cn (X.X.); jjwu@jiangnan.edu.cn (J.W.); yulin@jiangnan.edu.cn (L.Y.)

² Jiangsu Provincial Research Center of Light Industrial Opto-Electronic Engineering and Technology, Wuxi 214122, China

³ Key Laboratory of Electro-Optical Countermeasures Test & Evaluation Technology, Luoyang 471003, China; 6211205007@stu.jiangnan.edu.cn

* Correspondence: yanghuang@jiangnan.edu.cn

Abstract: To overcome the atmospheric turbulence aberration, and improve the quality of light beam in visible light communication (VLC), a compact 69-element deformable mirror (DM) using micro voice coil actuators was designed based on systematic theoretical analysis. The structural parameters of the micro voice coil actuator were optimized by electromagnetic theory and the finite element method. The DM was optimized from the aspects of thermal deformation, response time, coupling coefficient, and other parameters. Finally, wavefront fitting and residual calculation were completed according to the influence function. The optimized voice coil deformable mirror (VCDM) has a large phase stroke, good thermal stability, a short response time of less than 0.7 ms, and a large first resonance of 2045 Hz. The fitting residuals of the VCDM for the first 10 Zernike modes with a PV value of 8 μm are all below 10 nm (RMS). Compared with a similar DM, the obtained results from our compact VCDM indicate that it has a higher wavefront fitting precision. VCDM corrected complex random aberrations in the VLC scenario and improved the coupling efficiency of the signal beam, proving that the compact VCDM with high performance and low cost has a good application prospect in VLC systems.



Citation: Jiang, L.; Hu, L.; Hu, Q.; Xu, X.; Wu, J.; Yu, L.; Huang, Y.

Sixty-Nine-Element Voice Coil Deformable Mirror for Visible Light Communication. *Photonics* **2023**, *10*, 322. <https://doi.org/10.3390/photronics10030322>

Received: 23 February 2023

Revised: 13 March 2023

Accepted: 14 March 2023

Published: 17 March 2023



Copyright: © 2023 by the authors. Licensee MDPI, Basel, Switzerland. This article is an open access article distributed under the terms and conditions of the Creative Commons Attribution (CC BY) license (<https://creativecommons.org/licenses/by/4.0/>).

Keywords: visible light communication; phase modulation; deformable mirror; voice coil actuator

1. Introduction

Visible light communication (VLC) can provide much higher transmission rates than traditional wireless communication systems. Only the light-field distribution and spatial characteristics of LED or LD devices are considered in current VLC research. However, the actual VLC system channels include many factors, such as receiver frequency response characteristics, optical antennas, atmospheric turbulence, background light noise, diffraction, and so on [1]. Atmospheric turbulence will deteriorate the quality of the light beam, and introduce optical aberrations, which decreases the signal-to-noise ratio (SNR) of the light signal. To solve the problem, the deformable mirror (DM) in an adaptive optics system is used to correct the aberration introduced by atmospheric turbulence [2–4].

In 1972, J. Y. Hardy used adaptive optics in laser communication to correct atmospheric turbulence. In 1974, they completed a horizontal transmission path experiment of more than 300 m [5]. Although the traditional phase conjugate adaptive optics technology works well in short-distance laser communication, it encounters many challenges in long-distance transmission. Experiments by C. A. Primmerman on a 5.5 km horizontal transmission path show that the correction effect decreases with increasing scintillation [6]. Deformable mirrors with higher wavefront fitting precision can improve this problem. However, the coupling coefficient of a traditional VCDM is generally larger than 60%, much larger than

piezoelectric (PZT) DM. For a compact VCDM, a relatively small coupling coefficient is valuable to obtain a high wavefront correction precision. In addition, it should be noted that it is expensive using custom-developed VCDM with complex structures for astronomical observations. In applications, such as retinal imaging, biological microscope, and optical communication, a compact and relatively inexpensive DM with high electro-optical performance is necessary.

Different kinds of DMs have been investigated, such as PZT DM [7], magnetic fluid DM [8], electrostatic DM [9], micro-electro-mechanical system (MEMS) DM [10,11], and voice coil DM (VCDM) [12,13]. Furthermore, several DMs specially used for laser communication have been investigated. K. Ahn proposed a CVD SiC DM with monolithic cooling channels. The faceplate is 200 mm in diameter and 3 mm in thickness, and it is actuated by 137 stack-type PZT transducers arranged in a square grid [14]. V. Toporovsky developed a Water-cooled stacked-actuator flexible mirror for high-power laser beam correction. The deformable mirror has a diameter of 120 mm and 121 piezo actuators in a hexagonal arrangement [15]. Compared to PZT DMs, VCDMs have the merits of low driving voltage and linear response. However, standard VCDMs have two obvious drawbacks: (1) large coil diameter with a high cost that cannot be used in a compact VCDM, (2) high coupling coefficient that is difficult to correct high-order aberrations. In the paper, an alternative compact VCDM is presented by deriving theoretical equations that could guide a reasonable design. The designed micro voice coil actuator (VCA) has a small diameter of about 2 mm, only about a tenth of a standard one, which allows a compact VCDM with a high density of actuators. To decrease its coupling coefficient and power dissipation and improve its electro-optical performances, the VCDM's structure is simplified and optimized based on analyzing factors that affect its electro-optical performances, such as resonant frequency, power dissipation, coupling coefficient, response time, and so on. In fact, these parameters are influenced by the interactions among multi-physical fields, such as electromagnetic, thermal, stress, and strain fields. For example, increasing the current in a voice coil can produce a large electromagnetic force and increase its phase stroke. However, it can also lead to a large thermal dissipation, and even distort VCDM's thin mirror. Therefore, theoretical mathematical equations were derived to find the reasonable relationship among them and the reasonable requirement from the applications' point of view. Further, numerical simulations based on the finite element method were used to optimize the compact VCDM.

In the paper, the compact VCDM with high electro-optical performance is designed theoretically and demonstrated. In Section 2, a theoretical analysis is given according to their typical applications. In Section 3, its structure is designed, and its micro VCA is optimized based on electromagnetic finite element theory. In Section 4, the temporal and spatial properties of the compact VCDM using optimized micro VCA are discussed and compared with available DM in our lab. Finally, conclusions are given in Section 5.

2. Theory

There are many factors that affect the electro-optical performance of a compact VCDM, such as the electromagnetic force of micro VCA, power dissipation and efficiency of micro VCA, response time of VCDM, and fitting error. DM with only one or two of them with excellent values as reported in references could not really lead to a high electro-optical performance for a compact VCDM. Therefore, it is necessary to analyze systematically the requirements from the application's point of view and the relationships among them according to electromagnetic theory.

2.1. Electromagnetic Force of Micro VCA

The amplitude of electromagnetic force outputted by micro VCA is one of the key factors that determine the phase stroke of VCDM. In addition, the parameters of the structure and the external conditions including the current and the cooling element should also be considered [16]. Micro VCA as shown in Figure 1 eliminates the mechanical connection between the stationary part and the moving part of an actuator through electromagnetic

forces. It includes a thin mirror, springs, struts, a permanent magnet, and a coil from top to bottom. The geometry of the micro VCA is cylindrical. In addition, r_m is the magnet's radius, h_m is the magnet's height, d_{c-in} is the coil's inner diameter, d_{c-out} is the coil's outer diameter, h_c is the coil's height, and h_g is the height of the air gap.

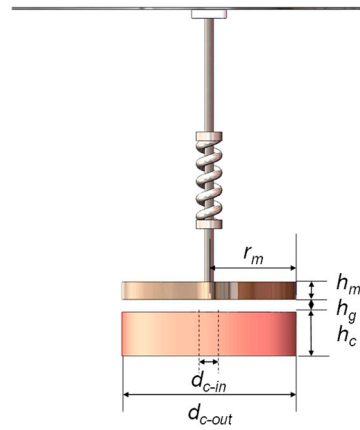


Figure 1. Structure of micro VCA.

The mathematical relation between output force and structural parameters of micro VCA could be derived according to the Biot-Savart law. The field vector H of the current-carrying coil at the position vector r is

$$H = \frac{B}{\mu_0} = \frac{\int_L \frac{\mu_0}{4\pi} \frac{Idl \times e_r}{r^2}}{\mu_0} = \int_L \frac{1}{4\pi} \frac{Idl \times e_r}{r^2}, \tag{1}$$

where μ_0 is vacuum magnetic permeability, Idl is the current element, and e_r is the unit vector along a position vector r . The permanent magnet in the VCA is in the magnetic field generated by the current-carrying coil, so the electromagnetic force can be expressed as

$$F = \int_V B_r \nabla H dv = \int_V B_r \nabla \int_L \frac{1}{4\pi} \frac{Idl \times e_r}{r^2} dv, \tag{2}$$

where V is the volume of a permanent magnet, and B_r is the remanence of the permanent magnet.

From Equation (2), it is obvious that the factors that affect the electromagnetic force of a micro VCA include the following factors: (1) remanence that depends on the material of a magnet; (2) surface magnetism of the permanent magnet, and it is related to the magnetization direction and size of the magnet; (3) the current through the coil; (4) the geometrical size of the coil; (5) the distance between the magnet and the coil, that is, the air gap of the micro VCA. The accurate optimization of micro VCA is based on the finite element analysis of the electromagnetic field.

2.2. Power Dissipation and Efficiency of Micro VCA

To quantify the performance of the micro VCA, the efficiency ε as the factor of metrics is used [17]. It is defined as

$$\varepsilon = \frac{F}{\sqrt{P}}. \tag{3}$$

In Equation (3), the unit of ε is $N/W^{1/2}$, F is the electromagnetic force, and P is the power dissipation of the micro VCA that is equal to I^2R . From Equations (2) and (3), ε could be written as

$$\varepsilon = \frac{F}{\sqrt{I^2R}} = \int_V B_r \cdot \nabla \int_L \frac{1}{4\pi} \frac{dl \times e_r}{r^2 \sqrt{R}} dv. \tag{4}$$

According to Equation (4), the efficiency is a physical quantity independent of the coil current, evaluating the structural parameters of the actuator. A larger value of efficiency means that VCA could generate a larger force with less power dissipation. Therefore, the larger the efficiency of VCA is, the better VCA will be.

The optimized VCA is also assembled into the DM for thermal analysis. Meanwhile, the response speed of the DM is also very important, so it is necessary to carry out a force-velocity analysis of the VCA and a modal analysis of the mirror. Finally, the statics of the mirror is analyzed, and the influence function related to the correction ability is obtained.

2.3. Response Time of VCDM

The optical communication system requires DM with fast response speed because the temporal error will deteriorate the compensation effects. The frequency of atmospheric turbulence aberrations is much faster than that in the eye [18]. The bandwidth of the VCDM should meet the atmospheric turbulence wavefront correction. The Greenwood frequency f_c related to the required control bandwidth of an AO system is [19]

$$f_c = \left[0.0196(k/\sigma_r)^2 \int_0^L C_n^2(z)v^{5/3}(z)dz \right]^{3/5}, \tag{5}$$

where $k = 2\pi/\lambda$, λ is the wavelength, σ_r is the uncorrected power, L is the path length, $C_n^2(z)$ is the refractive-index structure constant, and $v(z)$ is the wind speed. For a single turbulence layer with constant wind speed v , the Greenwood frequency can be approximated as

$$f_c = 0.43 \frac{v}{r_0}. \tag{6}$$

For strong atmospheric turbulence with wind speed v of 10 m/s and r_0 of 5 cm, the Greenwood frequency is approximately 86 Hz. The operating bandwidth of the DM is limited by several factors including the response time of the VCA and the first mechanical resonance frequency of the mirror. With 100 Hz operating bandwidth as a goal, the response time of the actuator should be less than 5 ms and the first resonance frequency of the mirror is aimed at 2000 Hz.

2.4. Fitting Error of VCDM

The fitting error of DM directly affects the performance of the adaptive optics system. The fitting error σ_{fit} arises from the limited number of actuators of the DM and thus the limited number of spatial frequencies that it can correct. The variance of the fitting error can be approximated by [20]:

$$\sigma_{fit}^2 = \kappa D \left(\frac{\sqrt{\pi/N}}{r_0} \right)^{5/3} \tag{7}$$

where κ is the fitting error coefficient, depending on the type of mirror that is used. For continuous face-sheet DM, κ is equal to 0.14. D is receiving the aperture. N is the number of actuators, which in this paper is 69; and r_0 is the Fried parameter, generally ranging from 5 cm to 20 cm.

3. Design and Optimization

3.1. Model of Compact VCDM

The exploded 3D drawing for the model of a 69-element compact VCDM is shown in Figure 2. The structure of compact VCDM mainly includes ten components listed in Table 1. The pupil diameter in the front shell is 17 mm. The diameter of the thin mirror is 24 mm and is mounted on the O-ring. 69 micro VCAs are mounted on the substrate. The inter-actuator distance is 2.5 mm and the diameter of the substrate is 26 mm. A cylindrical micro VCA contains a permanent magnet and a voice coil. One end of the strut is attached to a micro

VCA, while the other is attached to the back of the thin mirror. The strut transmits the force of an actuator to the thin mirror and deforms the local surface of the thin mirror. The shaft of a strut is mounted with a spring in the spring-fixing plate. This structure provides the micro VCA with axial stiffness, which overcomes the problem that an actuator’s mover is directly suspended on the mirror in traditional VCDMs [21].

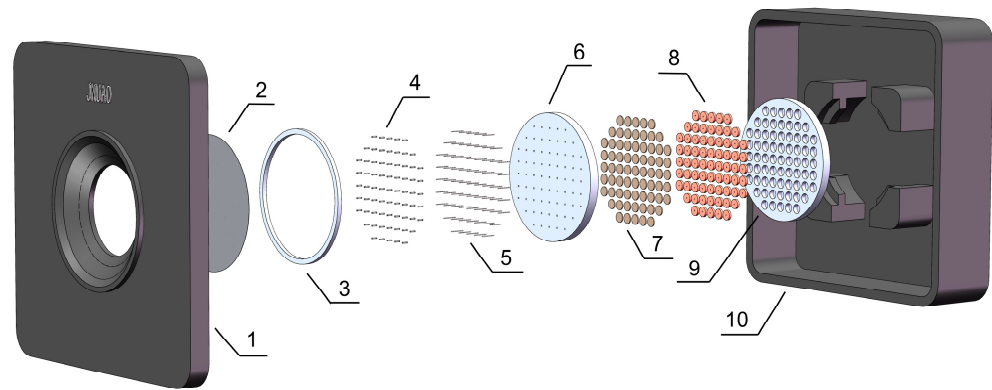


Figure 2. 3D drawing of VCDM. Front shell 1, thin mirror 2, O-ring 3, springs 4, struts 5, spring fixing plate 6, permanent magnets 7, voice coils 8, substrate 9, back shell 10.

Table 1. The composition of compact VCDM.

Serial Number	Component
1	Front shell
2	Thin mirror
3	O-ring
4	Springs
5	Struts
6	Spring fixing plate
7	Permanent magnets
8	Voice coils
9	Substrate
10	Back shell

3.2. Optimization of Micro VCA

To realize the compact VCDM, the pitch of actuators must be small enough. The geometrical shape of the VCA array as shown in Figure 2 is square with a pitch of 2.5 mm. In addition, the diameter of the micro VCA is less than 2.5 mm. The geometrical model of VCA is built and analyzed with Ansys software. The initial geometrical sizes for the micro VCA are defined as follows: (1) the permanent magnet with a radius of 1 mm and height of 0.1 mm; (2) the coil with an inner diameter of 0.2 mm, the outer diameter of 2.2 mm, and a height of 1 mm. When the permanent magnet moves to the side close to the coil, it is necessary to avoid touching the coil, that is, the height of the air gap should be larger than the mechanical stroke of the micro VCA. So, the initial size of the air gap is 50 μm . The permanent magnet is made of NdFe35. The parameters that need to be optimized are listed in Table 2.

Table 2. Parameters for micro VCAs to be optimized.

Parameters	Unit	Values	Step
Magnet radius	[mm]	$0.1 \leq r_m \leq 1.1$	0.1
Magnet height	[mm]	$0.05 \leq h_m \leq 1$	0.05
Coil inner diameter	[mm]	$0.2 \leq d_{c-in} \leq 1$	0.2
Coil outer diameter	[mm]	$0.4 \leq d_{c-out} \leq 2.2$	0.2
Coil height	[mm]	$0.1 \leq h_c \leq 1$	0.1
Air gap	[μm]	$50 \leq h_g \leq 100$	10

For two different magnetization directions of permanent magnets, the effect of electromagnetic force as a function of current is shown in Figure 3. The results indicate that there is a linear relationship between the electromagnetic force and the inputted current for permanent magnets with both axial magnetization (black square in Figure 3) and radial one (red triangle in Figure 3), which could be explained with Equation (2). For the same current, the force under radial magnetization is larger than that under axial one. Additionally, the former is larger by a factor of 1.5.

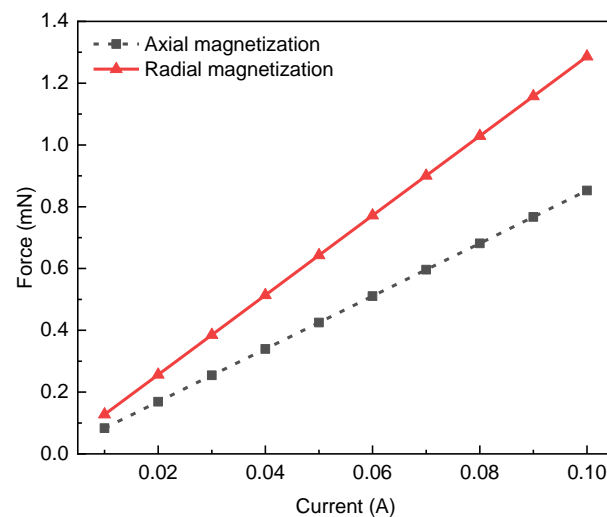


Figure 3. The electromagnetic force of VCA is a function of current for different magnetization directions of the permanent magnet.

Figure 4a,b show the electromagnetic force and efficiency ϵ as a function of magnet radius and height, respectively. The larger the magnet radius and magnet height are, the larger the electromagnetic force and efficiency would be. Their differences are the curve slopes of the electromagnetic force and efficiency. It should be noted that the permanent magnet is the mover of VCA, and increasing the permanent magnet’s volume will reduce the response speed of VCA. Therefore, the optimized radius of the magnet is selected as 1 mm and its optimized height is selected as 0.2 mm. The results in Figure 4c indicate that as the inner diameter of the coil increases, both the electromagnetic force and the efficiency decrease. Therefore, the optimized inner diameter of the coil is 0.2 mm. Similarly, according to Figure 4d, the optimized outer diameter of the coil is 2 mm. The change of force and efficiency in Figure 4e is slightly different from the others. Although the electromagnetic force increases with the height of the coil, its efficiency first increases and then decreases. It is because the wire far away from the permanent magnet contributes less to the electromagnetic force. Considering the efficiency of the actuator, the optimized coil height is 0.4 mm. Figure 4f shows that the larger the air gap is, the smaller the electromagnetic force and efficiency are. Therefore, the optimized air gap of the micro VCA is 50 μm . In summary, after optimization, the micro VCA has a diameter of 2 mm and a height of 0.65 mm.

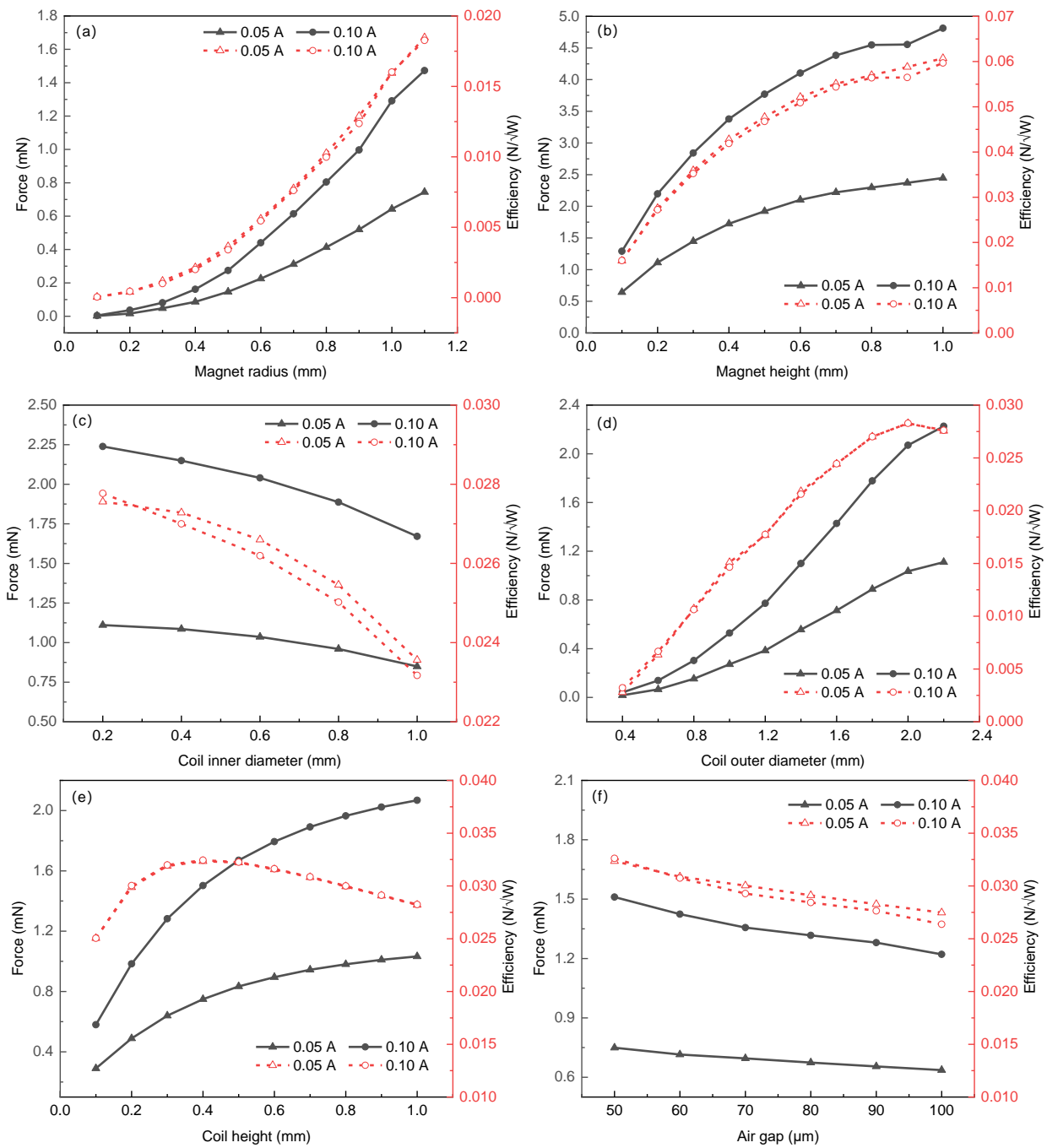


Figure 4. Force and efficiency as a function of VCA’s structural parameters. (a) Permanent magnet radius. (b) Permanent magnet height. (c) Coil inner diameter. (d) Coil outer diameter. (e) Coil height. (f) Air gap.

Figure 5a shows electromagnetic force and efficiency as a function of current before and after optimization. The obtained results indicate that the electromagnetic force and efficiency are increased after optimization. The output electromagnetic force of the VCA with optimized structural parameters is increased by a factor of 10%. The results in Figure 5b confirm that the efficiency is also increased obviously. The efficiency of the optimized VCA is up to $0.032 \text{ N/W}^{1/2}$.

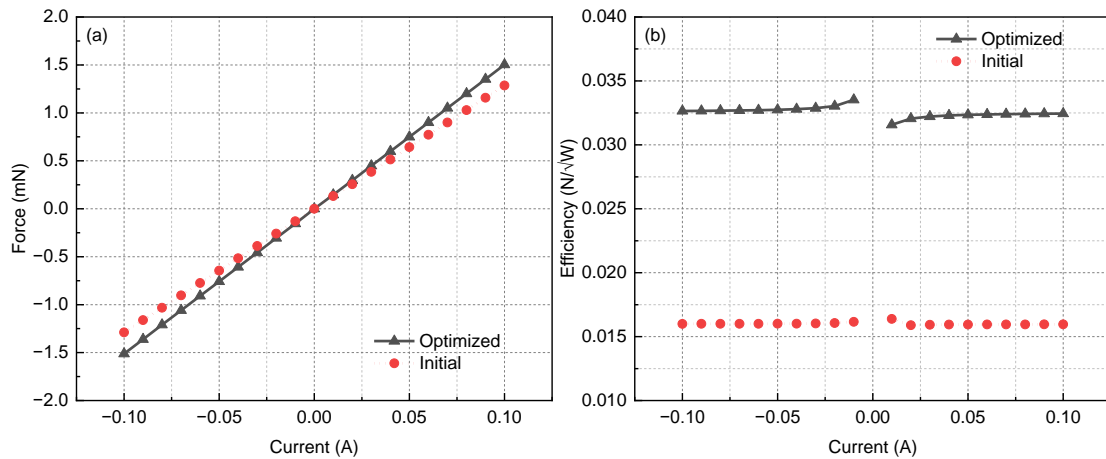


Figure 5. Electromagnetic force and efficiency as a function of current. The red circle is before optimization, and the black triangle is after optimization. (a) Force. (b) efficiency.

4. Discussion

4.1. Aberration of the Thin Mirror Due to Thermal Effect

To investigate the effect of temperature rise due to the current in VCAs on the thin mirror, the model of VCA is analyzed using Maxwell and steady-state thermal modules in Ansys software. The procedure of thermal analysis is shown in Figure 6.

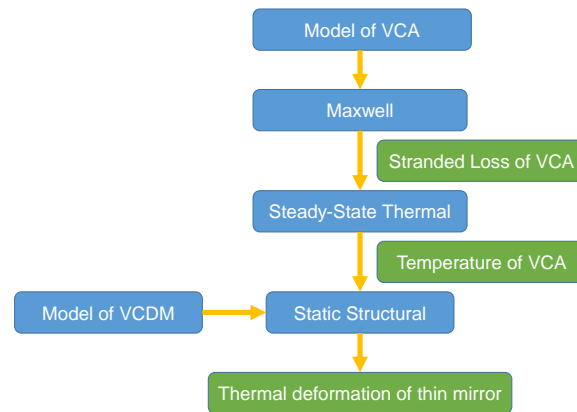


Figure 6. The thermal analysis process of the VCDM.

In compact DMs, active cooling elements, such as air cooling and water cooling, are generally not used. The thermal convection of all parts in VCDM is through the air. In the ANSYS Steady-State Thermal module, the air convection heat transfer coefficient is set to 5 W/(m²K) [22]. According to the mechanical model of the VCDM, as shown in Figure 2, the internal heat generation of the voice coil is introduced by the ohmic loss calculated by the Maxwell module. After that, the thin mirror temperature obtained by the Steady-State Thermal module is transferred to the Static Structural module to calculate the thermal deformation of the thin mirror.

The mirror material is CP1 Polyimide from NeXolve [23]. O-rings, springs, and struts are made of 316 Stainless Steel. The adhesive between the struts and the mirror is FR-4 Epoxy. The material of the permanent magnet is NdFe35, and the material of the coil is copper. To accelerate heat dissipation, the shell of the DM, spring fixing plate, and baseplate are all made of aluminum alloy. The parameters of the adopted materials are listed in Table 3.

Table 3. Material parameters related to thermal analysis.

Material	Thermal Conductivity [W/m/°C]	Coefficient of Thermal Expansion [1/°C]	Density [kg/m ³]	Young's Modulus [Pa]	Poisson's Ratio [/]
CP1 Polyimide	0.25	5.1×10^{-5}	1540	2.1×10^9	0.34
316 Stainless Steel	13.44	1.478×10^{-5}	7954	1.95×10^{11}	0.25
FR-4 Epoxy	0.294	1.688×10^{-5}	1900	2.64×10^{10}	0.1543
NdFe35	7.7	3.2×10^{-6}	7450	1.6×10^8	0.24
Copper	112.1	1.999×10^{-5}	8267	9.995×10^{10}	0.345
Aluminum Alloy	114	2.3×10^{-5}	2770	7.1×10^{10}	0.33

Figure 7a shows the temperature of the VCDM's thin mirror as a function of currents. The maximum temperature of the mirror surface increases along with the current. When the current is 0.1 A corresponding to a current density of 10 A/mm², the temperature rise of the VCDM is about 1 Celsius degree. Figure 7b shows the thermal deformation of the thin mirror due to temperature-rising non-uniform distribution. It indicates that the peak-to-valley (PV) of the thin mirror deformation increases along with the current. When the current density is 6 A/mm² corresponding to 0.06 A, the PV is 12.36 nm, which is about 0.022λ for λ = 550 nm. The root mean square (RMS) value of the mirror deformation is around 0, and it gradually deviates from 0 as the current increases. Therefore, the maximum control current of a single VCA should not be larger than 0.06 A for good thermal stability. At this time, the temperature and the deformation of the thin mirror are shown in inserted figures of Figure 7a,b.

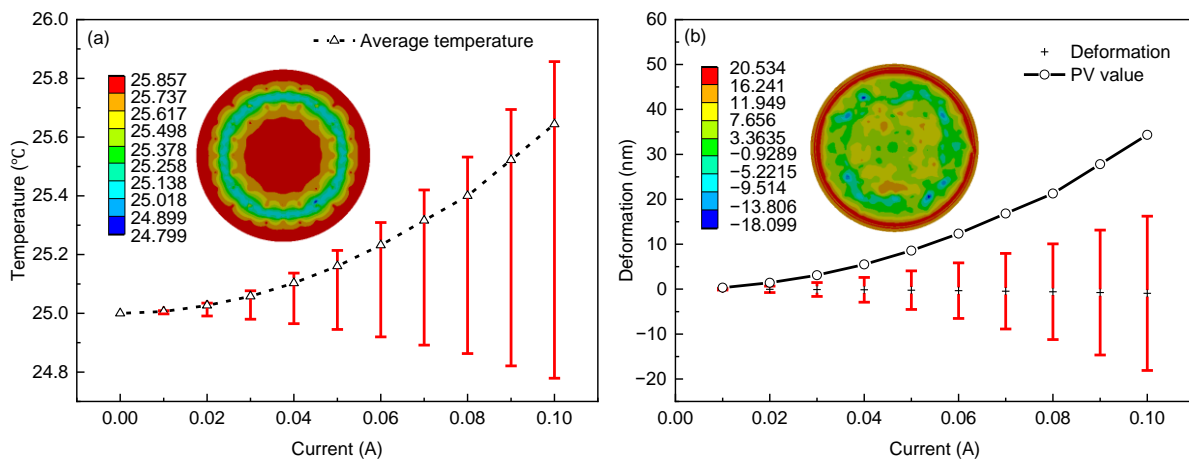


Figure 7. Temperature and thermal deformation of VCDM's thin mirror as a function of current. (a) The temperature of the thin mirror is a function of currents. The inset shows the temperature of the thin mirror when the current is 0.06 A. (b) The thermal deformation of the mirror surface as a function of currents. The inset shows the deformation of the thin mirror when the current is 0.06 A.

4.2. Response Time

For VCDM, our electromagnetic actuator development aims to increase its electromagnetic force and achieve a response speed as fast as possible [24]. The mass of the magnet mover is 4.6786 mg, and the initial velocity is 0 m/s. The response time of the VCA obtained using Maxwell is shown in Figure 8. The acceleration of the magnet mover is proportional to the current. All magnet movers can reach the set positions within 0.65 ms.

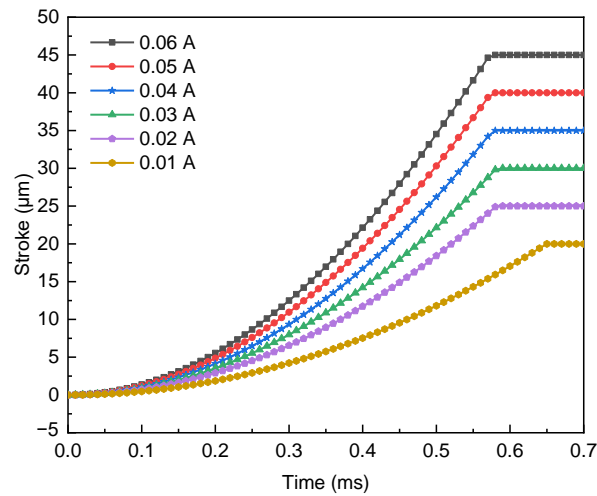


Figure 8. Time response of the VCA.

The first resonance frequency of the VCDM is mainly related to the mirror and the actuator stiffness. When the mirror material is selected, the mirror stiffness is determined by the mirror thickness. In addition, the stiffness of the VCA is dominated by the spring. As shown in Figure 9, the first resonance frequency is positively correlated with the spring stiffness for the same mirror thickness. However, large spring stiffness leads to a small electromagnetic force. Therefore, a mirror thickness ranging from 20 μm to 50 μm is preferable.

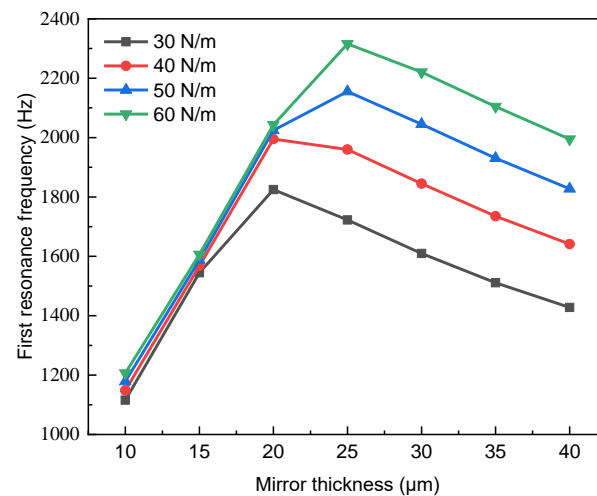


Figure 9. The first resonance frequency of the DM.

4.3. Wavefront Fitting Precision

The fitting precision of VCDM is directly related to its phase modulation ability. The influence function of VCDM could be expressed as [25]:

$$Z(r) = k \times \exp[\ln(\omega) \times \left(\frac{r}{d_0}\right)^\alpha], \tag{8}$$

where $Z(r)$ is the thin mirror deformation at a distance of r , k is the deformation of the mirror at the position of the central actuator, ω is the coupling coefficient that is the influence of the central actuator on neighboring actuators, the actuator spacing d_0 is 2.5 mm, and α is Gaussian index.

The coupling coefficient ω , a key indicator of the DM, is mainly influenced by the thickness of the mirror and the stiffness of the actuator. There is an optimum range of

coupling coefficients for a given DM, too large or too small will affect the performance of the system [26]. As shown in Figure 10, the coupling coefficient increases with mirror thickness. In addition, the larger the stiffness is, the smaller the coupling coefficient is.

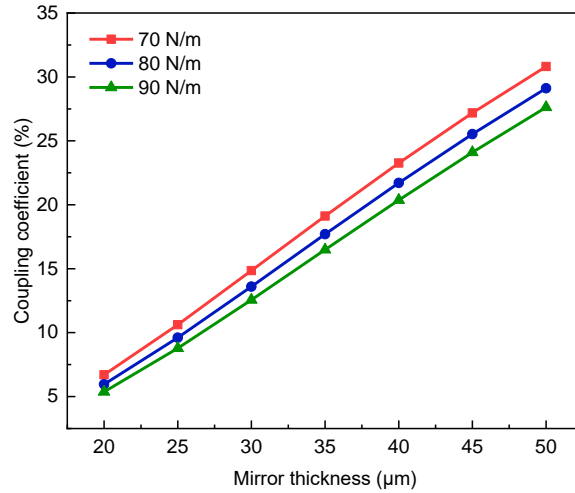


Figure 10. The coupling coefficient of the DM.

The wavefront fitting errors as a function of the coupling coefficient are shown in Figure 11 for four Zernike modes Z1, Z3, Z6, and Z10. The results indicate that with the increase of the coupling coefficient, errors decrease rapidly at first and then increase slowly. The optimal range of coupling coefficients for the compact VCDM is 23–28%, which is much smaller than that of a standard VCDM with a value larger than 60%. Generally, a relatively low coupling coefficient is preferable for high wavefront correction precision. To optimize the VCDM that meets the requirements further, we built four different VCDM models with 69 actuators as listed in Table 4. Their influence functions are shown in Figure 12.

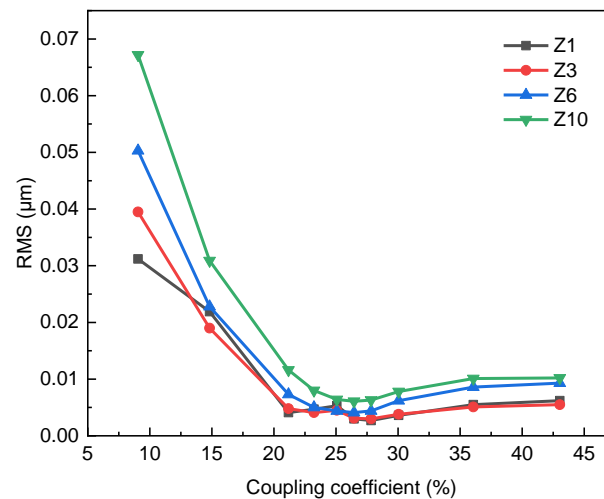


Figure 11. Correction ability to the coupling coefficient.

Table 4. Parameters of four patterns.

Pattern	Thickness	Stiffness	First Resonance	k	ω	α
P1	35 μm	55 N/m	2019.9 Hz	9.958	19.78%	2.191
P2	40 μm	61 N/m	2010.8 Hz	8.214	23.22%	2.111
P3	45 μm	70 N/m	2045.2 Hz	6.694	25.81%	2.049
P4	50 μm	80 N/m	2085.8 Hz	5.525	28.03%	1.995

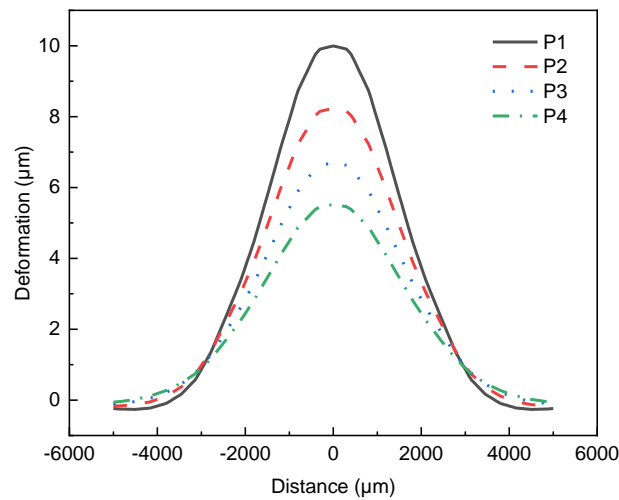


Figure 12. Influence functions of four patterns.

The MATLAB codes were programmed to complete the wavefront fitting and residual calculation according to the influence functions. The first 14 terms of the Zernike aberrations are fitted with four VCDM listed in Table 4. In the fitting experiment, four DMs are actuated to generate Zernike shapes with a PV value of 8 μm. Figure 13 shows the fitted wavefront and residuals of P3 for the 4th, 7th, 10th, and 13th Zernike modes. The results indicate that the fitting effect of P3 for some typical Zernike aberrations is less than 0.016λ . The results as shown in Figure 14 demonstrate the maximum phase stroke of P3. The tip or tilt stroke of P3 is up to 50 μm and the defocus stroke is about 30 μm. The experiment results are shown in Figure 15a. All four VCDMs listed in Table 4 fit the first 14 Zernike aberrations well, with a maximum RMS value of only 53 nm. P3 as the best VCDM is compared with DM69-25 from ALPAO S.A.S. The results in Figure 15b indicate that P3 has a better correction performance than the DM69-25, especially for Zernike aberrations that contain a defocus component. The fitting residuals of P3 for the first 10 Zernike modes with a PV value of 8 μm are all below 10 nm (RMS). Compared with the 121-element VCDM designed by Zhang Z. G., the wavefront fitting precision of P3 has increased by 13% [27].

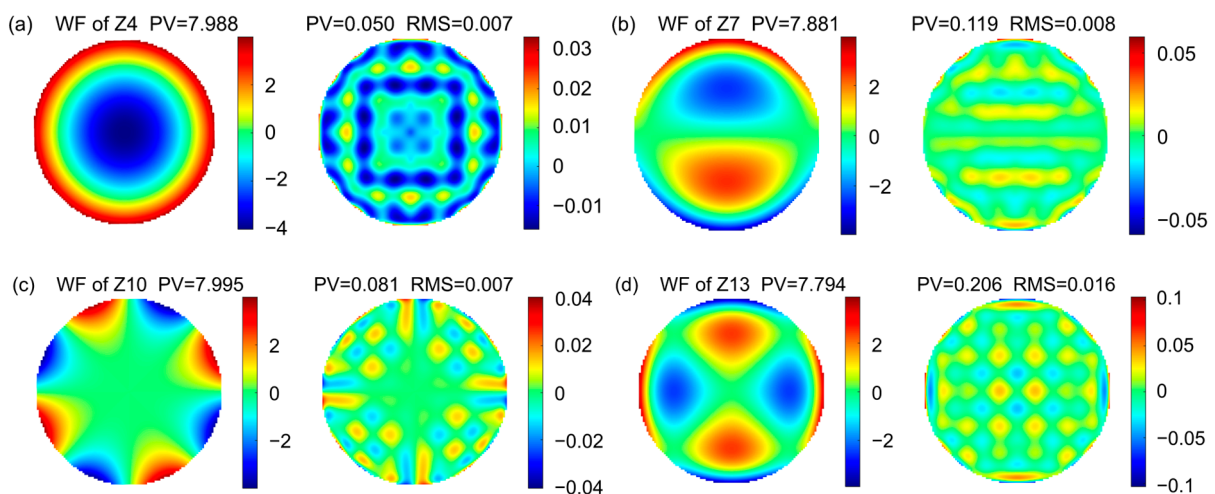


Figure 13. Wavefront Fitting and error of some typical Zernike modes. (a) The 4th Zernike mode Z4. (b) The 7th Zernike mode Z7. (c) The 10th Zernike mode Z10. (d) The 13th Zernike mode Z13.

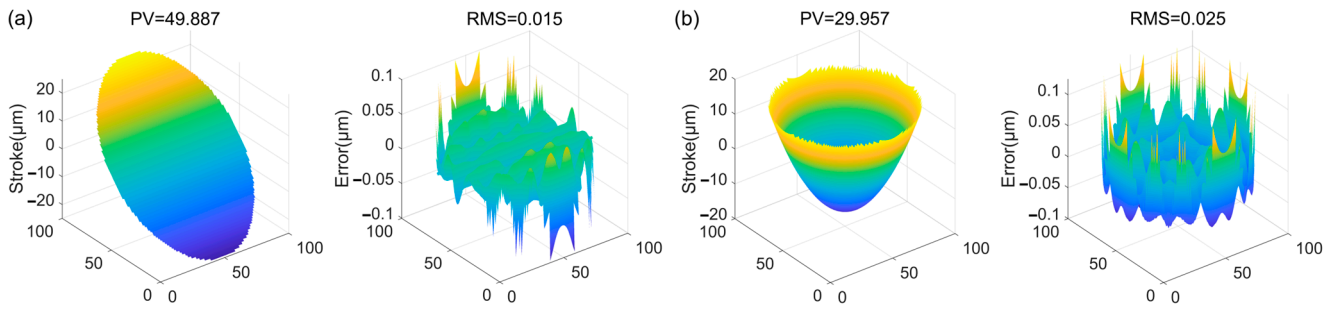


Figure 14. Stroke of P3. (a) Tip stroke. (b) Defocus stroke.

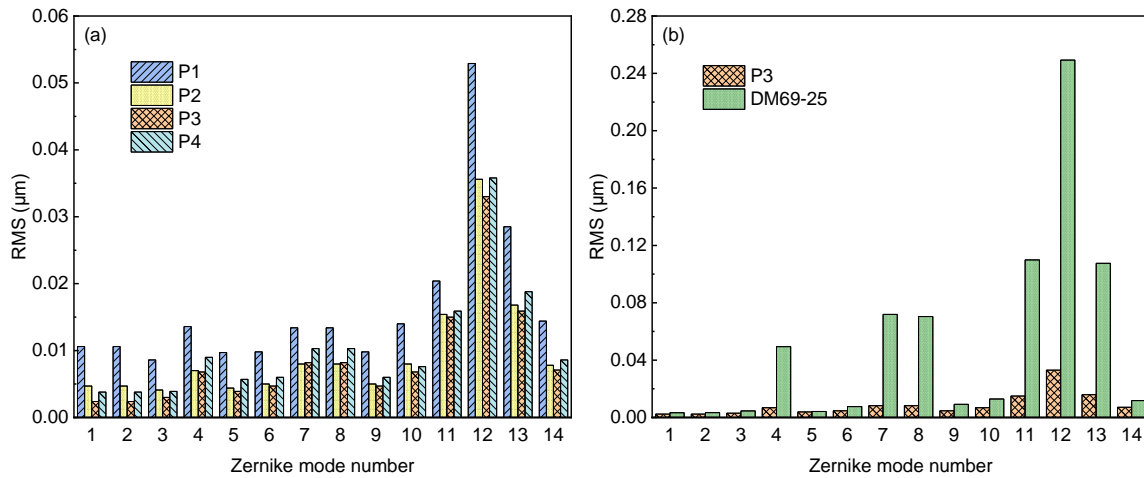


Figure 15. Fitting errors of the first 14 Zernike terms. (a) Comparison among four VCDMs listed in Table 4. (b) Comparison between P3 and DM69-25.

4.4. Application in Optical Communication

VCDM can compensate for wavefront distortion caused by atmospheric turbulence in wireless optical communication. Figure 16 shows the application of VCDM in an optical communication system. The beam is disturbed by atmospheric turbulence as it travels through free space. The light beam is coupled to the fiber by a lens at the receiving terminal. The coupling efficiency affects the bit error rate (BER). In free-space optical communication systems, it is necessary to improve the coupling efficiency to reduce the BER. An adaptive optics system is added in front of the coupling lens, and a VCDM P3 is used to compensate for the distorted wavefront. Given a signal beam wavelength of 650 nm, a VLC scenario is constructed. The communication method uses pulse-phase modulation, and the bit rate is 4 Gbps. The receiving aperture is 12 mm, and the mode field diameter is 8 μm. The comparison of the coupling coefficient before and after correction is shown in Figure 17. After correcting the complex random aberrations of the signal beam by VCDM, the coupling coefficient increases from 61.9%, 62.58%, 65.34%, 64.37%, 65.08%, 68.7% to 84.19%, 83.62%, 83.7%, 83.62%, 83.35%, and 83.57%, respectively. It shows that the VCDM P3 can effectively improve the coupling efficiency of the VLC system and reduce the BER.

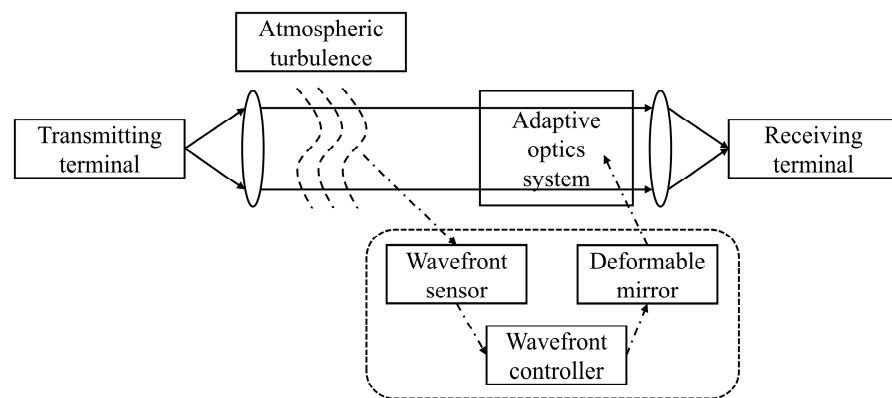


Figure 16. Application of VCDM in VLC system.

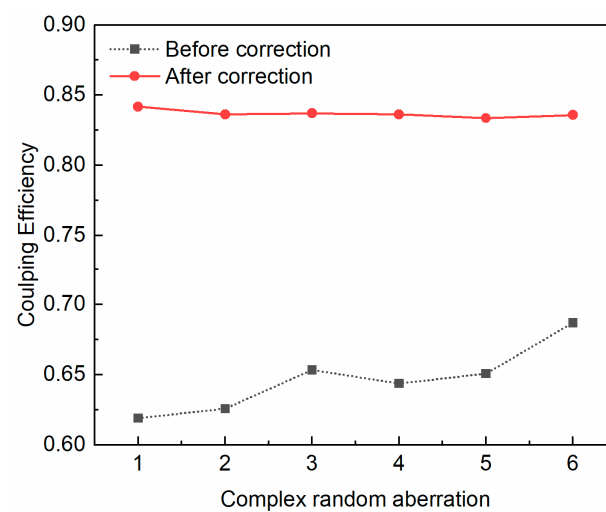


Figure 17. Comparison of coupling coefficients before and after aberration correction.

5. Conclusions

The VCDM has many merits, such as hysteresis free, low voltage, large phase stroke, and so on. However, traditional VCDM has many limitations and factors that hinder its use in visible-light communication systems. In the paper, to design a compact VCDM with high properties, the analytical expressions based on electromagnetic theory are given systematically, which include its parameters such as force, efficiency, and frequency, they guide the design and reasonable optimization of the compact VCDM. The thin mirror of the VCDM is made of polyimide and is coated with a thin layer of evaporated aluminum in order to make it optically reflective. The struts of micro VCAs are installed in the spring fixing plate, and the springs provide micro VCAs with axial stiffness. This structure makes it possible for the VCDM to have a higher operating bandwidth. Based on the multiparameter analysis and finite element analysis using ANSYS, a well-optimized VCDM is obtained with a micro VCA of a diameter of 2 mm and efficiency of $0.032 \text{ N/W}^{1/2}$. The maximum current of a micro VCA is 0.06 A, which makes the VCDM has excellent thermal stability. The temperature difference of the thin mirror is less than 0.4 degrees Celsius at the maximum current of 0.06 A, and the thermal deformation of the thin mirror is only 12.36 nm. The first resonance frequency of the 69-element compact VCDM is 2045 Hz which is more than three times that of the DM69-25. High wavefront fitting precision with a relatively low coupling coefficient of about 25% and large phase stroke is also demonstrated in the paper. The fitting results of Zernike aberrations show that the wavefront fitting precision of the compact VCDM has increased by 13% compared with a traditional VCDM. The VLC scenario was established, and the results proved that the compact VCDM can improve

the coupling efficiency. The above results indicate that the compact VCDM can satisfy the requirements of optical communication systems. The design and optimization method are also valuable for the design of other kinds of DMs. Our design decreases the development cost and obtains a compact VCDM with high electro-optical performance.

Author Contributions: Conceptualization, Y.H. and L.H.; methodology, Y.H. and L.J.; software, L.J.; validation, Y.H., L.H. and L.J.; formal analysis, X.X.; investigation, L.J.; resources, Q.H.; data curation, J.W. and L.Y.; writing—original draft preparation, L.J.; writing—review and editing, L.H.; visualization, L.J.; supervision, Y.H.; project administration, L.H.; funding acquisition, L.H. All authors have read and agreed to the published version of the manuscript.

Funding: This research was funded by the National Natural Science Foundation of China (No. 61475152, No. 62205127) and the Fund for Key Laboratory of Electro-Optical Countermeasures Test & Evaluation Technology (GKCP2021001).

Institutional Review Board Statement: Not applicable.

Informed Consent Statement: Not applicable.

Data Availability Statement: The data that support the findings of this study are available from the corresponding author upon reasonable request.

Conflicts of Interest: The authors declare no conflict of interest.

References

- Chi, N.; Zhou, Y.J.; Wei, Y.R.; Hu, F.C. Visible Light Communication in 6G: Advances, Challenges, and Prospects. *IEEE Veh. Technol. Mag.* **2020**, *15*, 93–102. [\[CrossRef\]](#)
- Rukosuev, A.; Nikitin, A.; Toporovsky, V.; Sheldakova, J.; Kudryashov, A. Real-Time Correction of a Laser Beam Wavefront Distorted by an Artificial Turbulent Heated Airflow. *Photonics* **2022**, *9*, 351. [\[CrossRef\]](#)
- Sabino, J.; Figueira, G.; Andre, P. Wavefront spatial-phase modulation in visible optical communications. *Microw. Opt. Technol. Lett.* **2017**, *59*, 1538–1541. [\[CrossRef\]](#)
- Yang, S.J.; Ke, X.Z. Experimental study on adaptive optical wavefront correction with dual mirrors in free space optical communication. *Optik* **2021**, *242*, 167146. [\[CrossRef\]](#)
- Hardy, J.W.; Lefebvre, J.E.; Koliopoulos, C.L. Real-time atmospheric compensation. *J. Opt. Soc. Am.* **1977**, *67*, 360–369. [\[CrossRef\]](#)
- Primmerman, C.A.; Murphy, D.V.; Page, D.A.; Zollars, B.G.; Barclay, H.T. Compensation of atmospheric optical distortion using a synthetic beacon. *Nature* **1991**, *353*, 141–143. [\[CrossRef\]](#)
- Toporovsky, V.; Kudryashov, A.; Skvortsov, A.; Rukosuev, A.; Samarkin, V.; Galaktionov, I. State-of-the-Art Technologies in Piezoelectric Deformable Mirror Design. *Photonics* **2022**, *9*, 321. [\[CrossRef\]](#)
- Wu, Z.Z.; Zhang, T.Y.; Mbemba, D.; Wang, Y.Y.; Wei, X.; Zhang, Z.; Iqbal, A. Wavefront sensorless aberration correction with magnetic fluid deformable mirror for laser focus control in optical tweezer system. *IEEE Trans. Magn.* **2021**, *57*, 1–6. [\[CrossRef\]](#)
- Kamel, A.; Kocer, S.; Mukhangaliyeva, L.; Saritas, R.; Gulsaran, A.; Elhady, A.; Basha, M.; Hajireza, P.; Yavuz, M.; Abdel-Rahman, E. Resonant adaptive MEMS mirror. *Actuators* **2022**, *11*, 224. [\[CrossRef\]](#)
- Bifano, T. ADAPTIVE IMAGING MEMS deformable mirrors. *Nat. Photonics* **2011**, *5*, 21–23. [\[CrossRef\]](#)
- Morgan, R.E.; Douglas, E.S.; Allan, G.W.; Bieren, P.; Chakrabarti, S.; Cook, T.; Egan, M.; Furesz, G.; Gubner, J.N.; Groff, T.D.; et al. MEMS deformable mirrors for space-based high-contrast imaging. *Micromachines* **2019**, *10*, 366. [\[CrossRef\]](#)
- Hamelinck, R.F.M.M. Adaptive Deformable Mirror: Based on Electromagnetic Actuators. Ph.D Thesis, Technische Universiteit Eindhoven, Eindhoven, The Netherlands, 22 June 2010.
- Liu, X.Y.; Cao, S.; Hu, D.T.; Ma, W.C.; Zhao, Z.Y.; Wu, J.J.; Zhu, H.X.; Su, Z.P.; Zhang, Y.X.; Hu, L.F. Design of voice-coil deformable mirror and its mechanical characteristics. *Chin. J. Liq. Cryst. Disp.* **2020**, *35*, 801–807. [\[CrossRef\]](#)
- Ahn, K.; Rhee, H.G.; Yang, H.S.; Kihm, H. CVD SiC deformable mirror with monolithic cooling channels. *Opt. Express* **2018**, *26*, 9724–9739. [\[CrossRef\]](#) [\[PubMed\]](#)
- Toporovsky, V.; Samarkin, V.; Sheldakova, J.; Rukosuev, A.; Kudryashov, A. Water-cooled stacked-actuator flexible mirror for high-power laser beam correction. *Opt. Laser Technol.* **2021**, *144*, 107427. [\[CrossRef\]](#)
- Wang, C.C.; Lu, S.Z.; Zhang, C.Y.; Gao, J.; Zhang, B.; Wang, S. Design and dynamic modeling of a 3-RPS compliant parallel robot driven by voice coil actuators. *Micromachines* **2021**, *12*, 1442. [\[CrossRef\]](#) [\[PubMed\]](#)
- Zhang, Z.G.; Hu, Q.L.; Ma, W.C.; Jiang, L.; Gu, H.; Wu, J.J.; Hu, L.F. Design and performance research of high efficiency variable reluctance voice coil actuator. *Chin. J. Liq. Cryst. Disp.* **2022**, *37*, 21–28. [\[CrossRef\]](#)
- Jarosz, J.; Mece, P.; Conan, J.M.; Petit, C.; Paques, M.; Meimon, S. High temporal resolution aberrometry in a 50-eye population and implications for adaptive optics error budget. *Biomed. Opt. Express* **2017**, *8*, 2088–2105. [\[CrossRef\]](#)
- Greenwood, D.P. Bandwidth specification for adaptive optics systems. *J. Opt. Soc. Am.* **1977**, *67*, 390–393. [\[CrossRef\]](#)
- Hardy, J.W.; Thompson, L. Adaptive optics for astronomical telescopes. *Phys. Today* **2000**, *53*, 69. [\[CrossRef\]](#)

21. Cugat, O.; Basrou, S.; Divoux, C.; Mounaix, P.; Reyne, G. Deformable magnetic mirror for adaptive optics: Technological aspects. *Sens. Actuator A-Phys.* **2001**, *89*, 1–9. [[CrossRef](#)]
22. Yu, E.; Joshi, Y.K. Natural convection air cooling of electronic components in partially open compact horizontal enclosures. *IEEE Trans. Compon. Packag. Technol.* **2000**, *23*, 14–22. [[CrossRef](#)]
23. Yin, J.J.; Mao, D.B.; Fan, B.; Bian, J.; Du, J.F. High dimensional stability polyimide membrane material for space optical imaging system. *Opto.-Electron. Eng.* **2021**, *48*, 210150. [[CrossRef](#)]
24. Plavec, E.; Petrinic, M.; Vidovic, M. Improving the force and time response of a DC solenoid electromagnetic actuator by changing the lower core angle. *J. Electromagn. Eng. Sci.* **2021**, *21*, 95–103. [[CrossRef](#)]
25. Huang, L.H.; Rao, C.H.; Jiang, W.H. Modified Gaussian influence function of deformable mirror actuators. *Opt. Express* **2008**, *16*, 108–114. [[CrossRef](#)] [[PubMed](#)]
26. Ahn, K.; Kihm, H. Moment actuator for correcting low-order aberrations of deformable mirrors. *Opt. Lasers Eng.* **2020**, *126*, 105864. [[CrossRef](#)]
27. Zhang, Z.G. *Structure Design and Performance Research of Modular Voice Coil Deformable Mirror*; Jiangnan University: Wuxi, China, 2022.

Disclaimer/Publisher’s Note: The statements, opinions and data contained in all publications are solely those of the individual author(s) and contributor(s) and not of MDPI and/or the editor(s). MDPI and/or the editor(s) disclaim responsibility for any injury to people or property resulting from any ideas, methods, instructions or products referred to in the content.